



## Quantification of non-algal light attenuation in the Sargasso Sea: Implications for biogeochemistry and remote sensing

DAVID A. SIEGEL\* and ANTHONY F. MICHAELS†

(Received 22 March 1995; in revised form 29 June 1995; accepted 14 August 1995)

**Abstract**—Observations of the diffuse attenuation coefficient spectrum ( $K_d(z,t,\lambda)$ ), made as part of the U.S. Joint Global Ocean Flux Study (JGOFS), Bermuda Atlantic Time-series Study (BATS), show significant seasonal variations that do not covary with the patterns in chlorophyll *a* concentrations. The spectral structure of these changes indicates that the variations in optical properties are caused by detrital particulate and/or colored dissolved organic materials. Multiple regression analyses over wavelength are used to deconvolve this “colored dissolved or detrital material” (CDM) signal from the chlorophyll signal. Generally, CDM light attenuation is nearly as large as the chlorophyll-related attenuation and it exhibits a seasonal signal related to changes in mixed-layer depth. In the winter, values of CDM are roughly uniform throughout the upper 150 m of the mixed layer, whereas in the summer significantly reduced CDM values are found in a shallow mixed layer with elevated values in the seasonal pycnocline. The summer-time pattern appears to be caused by the combination of reduction of CDM within the mixed layer by photo-oxidation and its production at depth. This seasonal cycle is different than that observed for dissolved organic or particulate organic carbon at BATS. Hence, optical inferences of CDM are not directly related to biogeochemically relevant materials, such as dissolved organic carbon. Quantification of the photon flux absorbed by CDM can be used to assess the role of CDM quanta absorption in photochemical transformations. We suggest that CDM-regulated rates of photo-oxidation play a critical role in the regulation of near-surface dimethyl sulfide concentrations on a seasonal timescale. Last, the existence of a strong CDM signal requires modification of the techniques used to estimate chlorophyll from satellite ocean color sensors. Copyright © 1996 Elsevier Science Ltd

### INTRODUCTION

Since Smith and Baker (1978a) coined the term “bio-optical properties”, quantitative linkages between optical and biological properties have been explored by many investigators with varying degrees of sophistication (e.g. Lorenzen, 1972; Smith and Baker, 1978a, 1978b; Atlas and Bannister, 1980; Prieur and Sathyendranath, 1981; Siegel and Dickey, 1987a; 1987b; Baker and Smith, 1982; Sathyendranath and Platt, 1988; Morel, 1988; 1991; Morel and Antoine, 1994; Bricaud *et al.*, 1995). For the most part, bio-optical parameterizations for the vertical attenuation of spectral downwelling irradiance, the diffuse attenuation coefficient spectrum ( $K_d(z,t,\lambda)$ ), have been expressed as a function of the algal pigment concentration (either the chlorophyll *a* (chl *a*) concentration alone or the sum of chl *a* and phaeopigment concentrations). One prominent exception to this is the work of Baker and Smith (1982) who modeled  $K_d(z,t,\lambda)$  as a function of both chl *a* and colored

\*Institute for Computational Earth System Science and Department of Geography, University of California at Santa Barbara, Santa Barbara, CA 93106, U.S.A.

†Bermuda Biological Station for Research Inc., Ferry Reach, GE 01, Bermuda.

dissolved organic carbon concentrations. Recently, Siegel *et al.* (1995a) have shown qualitatively that variations in  $K_d(z, t, \lambda)$  in the Sargasso Sea are due, in part, to materials other than algal pigments and that this “detrital-like” attenuation varies significantly on a seasonal timescale. Here, we quantify these observed CDM variations and address the biogeochemical and remote sensing implications of this component of light attenuation.

The diffuse attenuation coefficient spectrum can be approximately partitioned into components which describe the effects of different attenuating materials, or

$$K_d(z, t, \lambda) \cong K_w(\lambda) + K_{chl}(z, t, \lambda) + K_{other}(z, t, \lambda) \quad (1)$$

where  $K_w(\lambda)$  is the attenuation due to pure seawater (e.g. Smith and Baker, 1981),  $K_{chl}(z, t, \lambda)$  is the attenuation due to pigmented algal materials, and  $K_{other}(z, t, \lambda)$  corresponds to the attenuation due to non-algal materials in the water column (e.g. Blizard, 1986; Smith *et al.*, 1989). This partitioning assumes implicitly that the “quasi-inherency approximation” has been satisfied, i.e. that  $K_d(z, t, \lambda)$  is independent of variations in the geometry of the in-situ radiance distribution. This invariance of  $K_d(z, t, \lambda)$  has been verified approximately by both observations and numerical modeling (e.g. Baker and Smith, 1980; Siegel and Dickey, 1987a; Gordon, 1989).

The values of  $K_{other}(z, t, \lambda)$  and the composition of the materials that regulate  $K_{other}(z, t, \lambda)$  are poorly characterized (e.g. Blizard, 1986), in contrast to the well-understood regulation of  $K_{chl}(z, t, \lambda)$ . The composition and concentration of colored dissolved organic material (CDOM) and detrital particles contribute to values of  $K_{other}(z, t, \lambda)$  throughout the visible region of the spectrum (e.g. Kirk, 1994a). CDOM has been thought to be important in coastal regions, enclosed seas and near sources of terrigenous inputs (e.g. Jerlov, 1976; Bricaud *et al.*, 1981; Walsh *et al.*, 1992; Blough *et al.*, 1993; Kirk, 1994a). For the open sea, CDOM is generally considered unimportant. Many previous studies have compared CDOM observations at very high concentrations, such as in estuaries and coastal waters, with clearer open ocean regions. This comparison of the extreme cases leads to the conclusion that the open sea is for all practical purposes devoid of CDOM. Much work has been done on distributions of gelbstof (or CDOM) by optical oceanographers working within the Baltic Sea (e.g. Jerlov (1976) and references therein). They observed a strong inverse relationship between salinity and gelbstof concentration, leading them to conclude that oceanic waters have very low CDOM concentrations and that CDOM concentrations have a terrestrial origin. Detrital particulate materials also contribute to the absorption of visible radiation in the open ocean (e.g. Kishino *et al.*, 1984; Iturriaga and Siegel, 1989; Morrow *et al.*, 1989; Nelson and Robertson, 1993; Garver *et al.*, 1994). Observations from the Sargasso Sea have shown that detrital particle absorption is typically one-half of the total (e.g. Iturriaga and Siegel, 1989; Morrow *et al.*, 1989; Cleveland and Perry, 1994).

The spectral structure of CDOM and detrital absorption coefficients both can be characterized by an exponentially decreasing signal with wavelength (e.g. Bricaud *et al.*, 1981; Roesler *et al.*, 1989; Iturriaga and Siegel, 1989; Carder *et al.*, 1989, 1991; Blough *et al.*, 1993; Kirk, 1994a). For example, parameterizations of the CDOM absorption coefficient spectrum,  $a_{CDOM}(\lambda)$ , are typically of the form

$$a_{CDOM}(\lambda) = a_{CDOM}(\lambda_0) \exp(-S(\lambda - \lambda_0)) \quad (2)$$

where  $\lambda_0$  is a reference wavelength (440 nm) and  $S$  is the exponential slope. Values of  $S$  are roughly the same for detrital particles and CDOM, ranging from 0.010 to 0.020  $\text{nm}^{-1}$  (e.g.

Bricaud *et al.*, 1981; Carder *et al.*, 1989; Blough *et al.*, 1993; Hoge *et al.*, 1993; Kirk, 1994b). As the spectral structure for detrital particles and CDOM are approximately equal, it will be difficult to separate these components using optical means (Carder *et al.*, 1991). Hence, we will refer to the combined light attenuation due to CDOM and/or detrital particles as the "colored detrital material" or CDM signal.

In many bio-optical models, the phaeopigment concentration is used to separate algal from detrital absorption (e.g. Smith and Baker, 1978b; Soohoo and Kiefer, 1982; Kiefer and Soohoo, 1982; Cleveland and Perry, 1994). Fluorometric estimates of the phaeopigment concentration are confounded by the fluorescence of chlorophylls *b* and *c*. Hence, "corrected" estimates of phaeopigment concentrations in the oligotrophic ocean are typically very close to zero (e.g. Vernet and Lorenzen, 1987). Laboratory experiments using phytodetritus do not show clear relationships between detrital pigment concentrations and absorption coefficients (e.g. Nelson and Robertson, 1993). Hence, phaeopigment concentrations may not provide a useful means of determining detrital particulate attenuation and its variations for the open ocean.

Here, we use in-situ optical data from the Sargasso Sea to assess the magnitude of and variations in solar radiation attenuation by colored detrital materials. The data were sampled as part of the Bermuda Bio-Optics Project (BBOP; Siegel *et al.*, 1995a) and the JGOFS Bermuda Atlantic Time-series Study (BATS; Michaels *et al.*, 1994). The present focus is upon characterizing the variability in the diffuse attenuation coefficient spectrum,  $K_d(z, t, \lambda)$ , and to assess sources of its variations. First, we present the methods used to determine  $K_d(z, t, \lambda)$  and relevant biogeochemical properties sampled during the BATS program. We describe next the time-depth-spectral variability in  $K_d(z, t, \lambda)$ , and a statistical model is developed to partition  $K_d(z, t, \lambda)$  into algal and non-algal components. We conclude with a discussion of several of the implications of the patterns observed for the CDM light attenuation component.

## METHODS

The Bermuda Bio-Optics, Program (BBOP) is conducted in collaboration with the U.S. JGOFS Bermuda Atlantic Time-series Study (BATS) at a site 75 km south-east of Bermuda (in the vicinity of 31° 50'N; 64° 10'W). Biweekly-to-monthly BATS cruises commenced in October 1988 with 16–20 cruises conducted each year. The BBOP observations began in January 1992. The primary tool for BBOP is a profiling spectroradiometer (Biospherical Instruments, MER-2040, San Diego, CA; Smith *et al.*, 1984) which determines downwelling irradiance in eight different spectral wavebands (410, 441, 465, 488, 520, 565, 589, and 665 nm) and upwelling radiance in the same bands (plus 683 nm). Typically, the half power bandwidth of the spectral channels is 10 nm and the out-of-band response is better than 1 ppm (Siegel *et al.*, 1986). Only downwelling irradiance measurements,  $E_d(z, t, \lambda)$ , will be addressed in this paper. Several other instruments were interfaced with the spectroradiometer, including a SeaTech chlorophyll fluorometer, a SeaTech 25 cm beam transmissometer (660 nm), and SeaBird conductivity and temperature sensors. Profiles were made to 200 m. Incident spectral irradiance,  $E_d(0^+, t, \lambda)$ , was determined simultaneously from a mast-mounted spectroradiometer in 6 discrete wavebands (410, 441, 488, 520, 565 and 665 nm). All data were recorded on a ship-board computer at 4 Hz. Optical calibrations were performed every 4–6 months at UCSB where our irradiance standard has been directly traced to the National Institute of Standards and Technology (Mueller *et al.*, 1993).

The BBOP package is normally deployed off the stem A-frame of the R.V. *Weatherbird II*, ~3 m from the ship. During casts, the stem is oriented directly towards the sun to minimize ship shadowing (cf., Mueller and Austin, 1992). A detailed evaluation of the R.V. *Weatherbird II*'s shadow showed no significant effects on downwelling irradiance determinations and its derived products under our normal deployment scheme (Weir *et al.*, 1994). The R.V. *Cape Hatteras* was used for the first four months of 1993, and the effects of this larger vessel's shadow are unknown.

Data from the BBOP package were analyzed using an efficient data processing/documentation system that takes raw spectroradiometry data and performs a series of quality control/assessment procedures, filtering, and calculation procedures (Sorensen *et al.*, 1994; Siegel *et al.*, 1995b). The calculation of the diffuse attenuation coefficient spectrum,  $K_d(z,t,\lambda)$ , uses a robust least-squares regression over 10 1-m bins (Siegel *et al.*, 1995b). Final products for all parameters are 1 m binned fields of sampled and derived products. For this study,  $K_d(z,t,\lambda)$  estimates are subsampled at 5 m increments in the vertical. Processed spectroradiometry casts used in this study are available via anonymous ftp (ftp.icess.ucsb.edu, cd pub/BBOP/data).

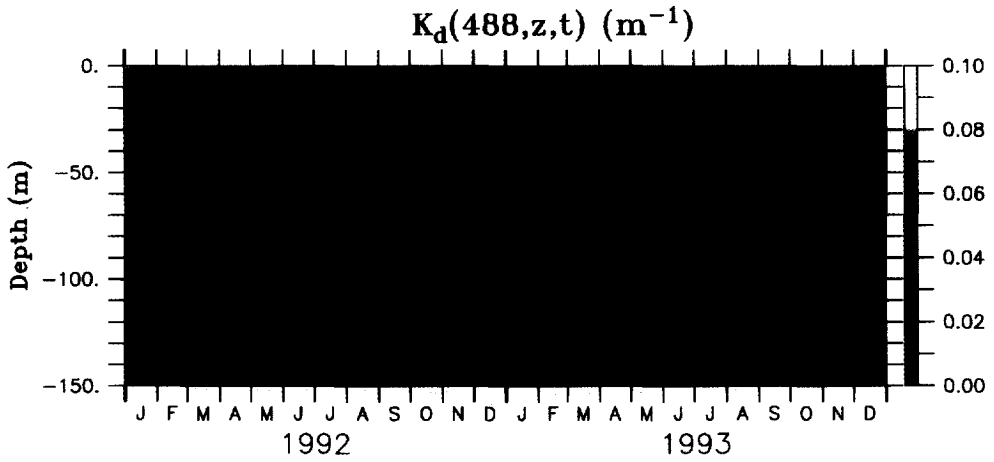
The biogeochemical data used in this paper were collected as part of the BATS program or as ancillary investigations on BATS cruises. The methods are described in methods manuals, data reports and publications (Knap *et al.*, 1993; Michaels *et al.*, 1994; Carlson *et al.*, 1994). Chlorophyll *a* was measured by both high precision liquid chromatography (HPLC) and fluorometric techniques. Particulate organic carbon (POC) was collected on pre-combusted Whatman GF/F filters (0.7  $\mu\text{m}$  nominal pore size) and measured by combustion in a CHN analyzer (Knap *et al.*, 1993). Dissolved organic carbon (DOC) was measured by high-temperature catalytic combustion and these data have been published elsewhere (Carlson *et al.*, 1994). Dimethyl sulfide (DMS) concentrations are determined by gas chromatography of cryofocussed, sparged samples; the methods and data will be published elsewhere (Dacey *et al.*, submitted).

## DATA AND RESULTS

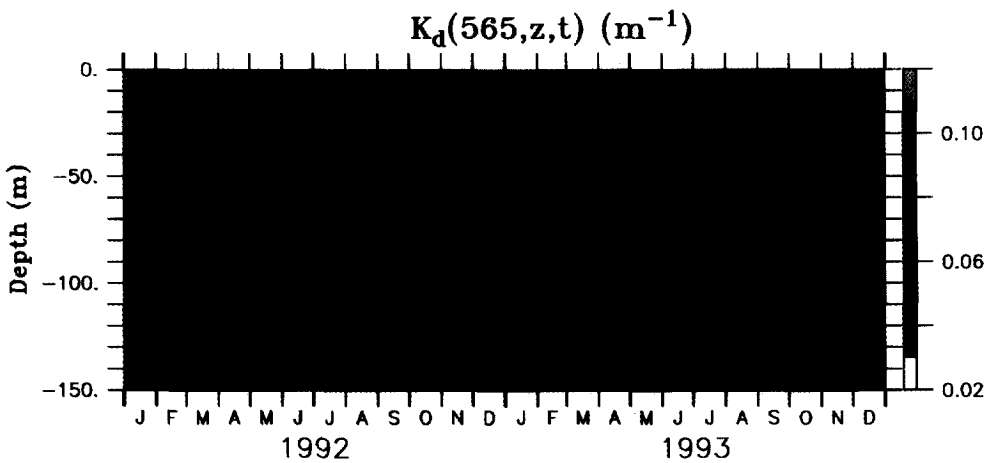
The time-space patterns of the diffuse attenuation coefficient for downwelling irradiance at 410, 441, and 488 nm,  $K_d(z,t,410)$ ,  $K_d(z,t,441)$  and  $K_d(z,t,488)$  are similar to each other (Fig. (a)–(c)) and to the chl *a* distribution (Fig. 1(e)). This is expected as  $K_d(z,t,\lambda)$  is often modeled as a simple function of the chl *a* concentration (e.g. Smith and Baker, 1978b; Siegel and Dickey, 1987b; Morel, 1988). The highest  $K_d(z,t,\lambda)$  values occur in the summer-to-fall seasons in an intense subsurface maximum that is coincident with the chl *a* maximum (Fig. 1(e)). Above the chlorophyll maximum, summer-time  $K_d(z,t,\lambda)$  values are at their lowest, at times less than solar radiation attenuation values reported for "pure" ocean water (see below). During each spring bloom, values of  $K_d(z,t,\lambda)$  are significantly elevated throughout the water column, although peak values are less than are observed within the subsurface maximum.

In general, the range of variability in  $K_d(z,t,\lambda)$  decreases with increasing wavelength. In particular, the time-depth pattern of  $K_d(z,t,565)$  (Fig. 1(d)) shows many of the same near-surface patterns as are observed in the blue-to-green  $K_d(z,t,\lambda)$  distributions, although a subsurface maximum is not observed. Below a depth of 100 m, the distribution of  $K_d(z,t,565)$  (Fig. 1(d)) decreases rapidly and values of  $K_d(z,t,565)$  approach those observed for the blue-green wavebands. This rapid drop-off in  $K_d(z,t,565)$  with depth is probably



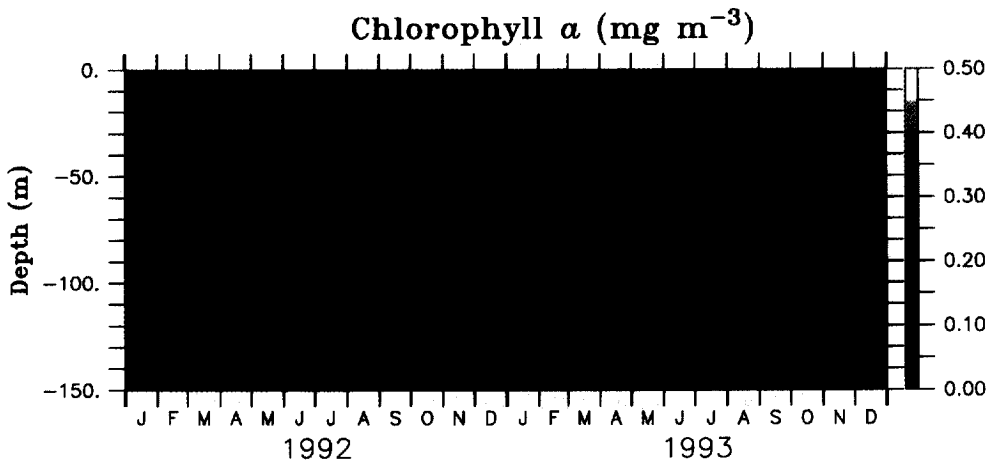


(c)

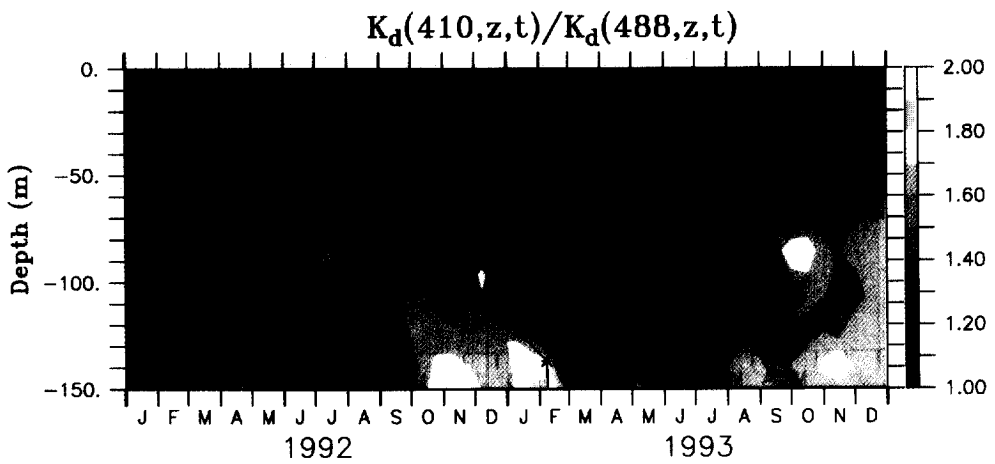


(d)

Fig. 1. (c) and (d)

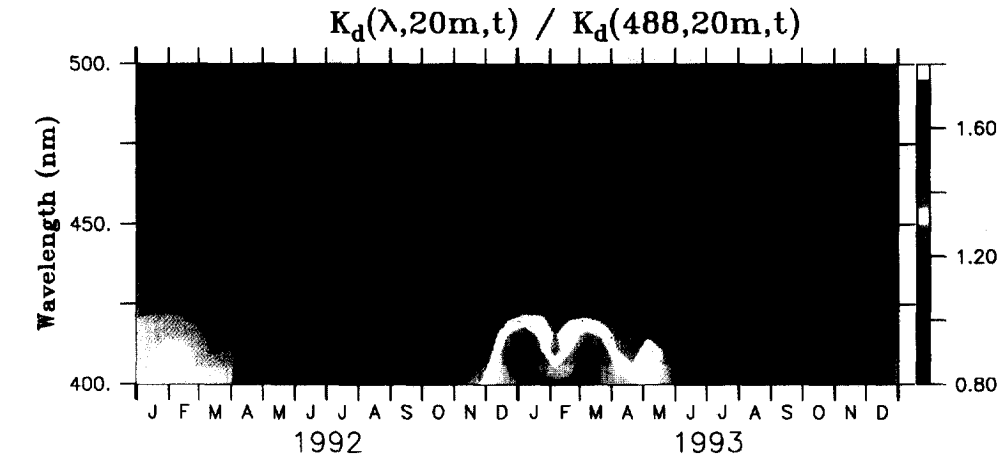


(e)

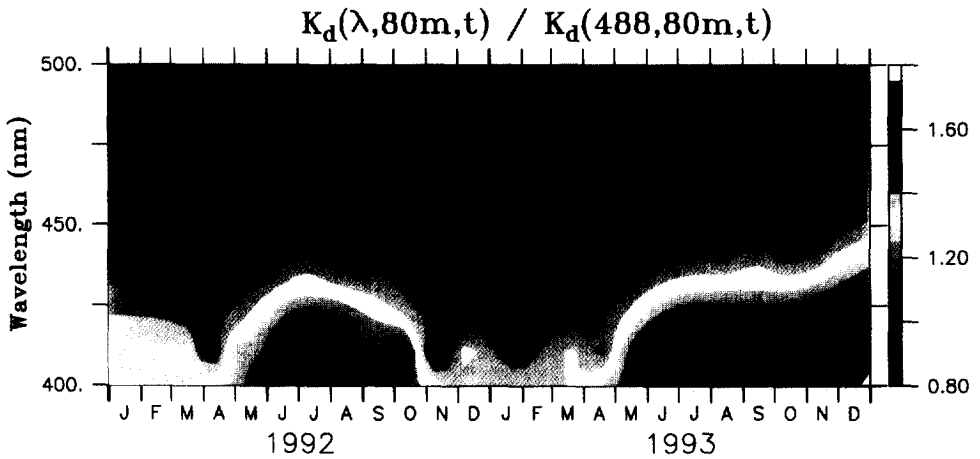


(f)

Fig. 1. (e) and (f)

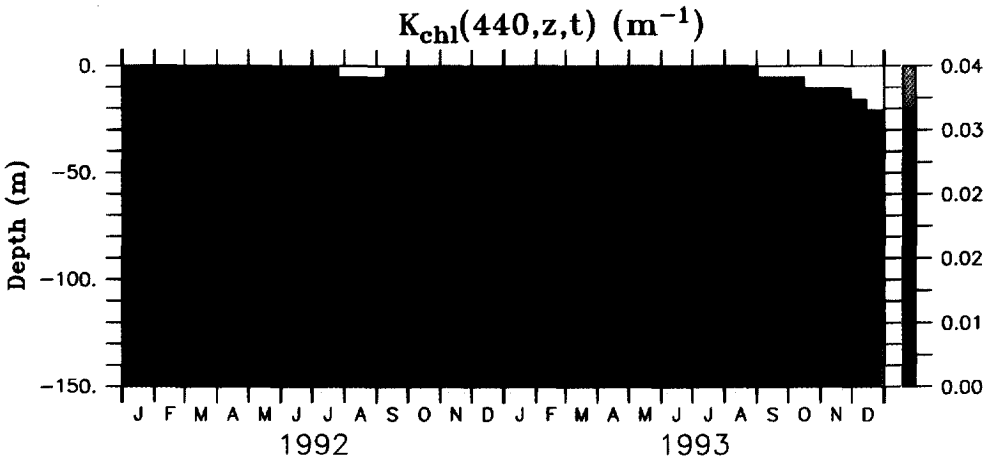


(a)

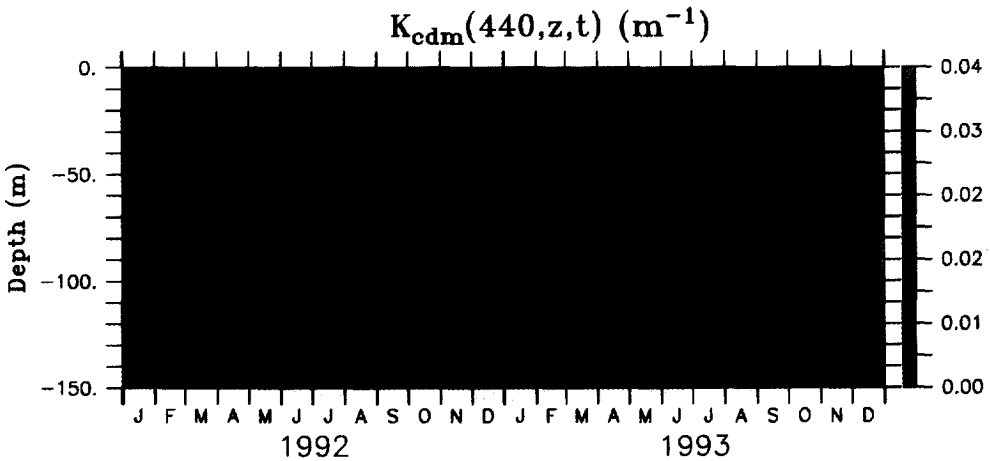


(b)

Fig. 4. Wavelength-time contours of normalized  $K_d(z_o, t, \lambda)$  spectra at fixed depths of (a) 20 m and (b) 80 m. The value of  $K_d(z_o, t, 488)$  is used as the normalization factor and spectral data from 410, 441, 465 and 488 nm are employed.

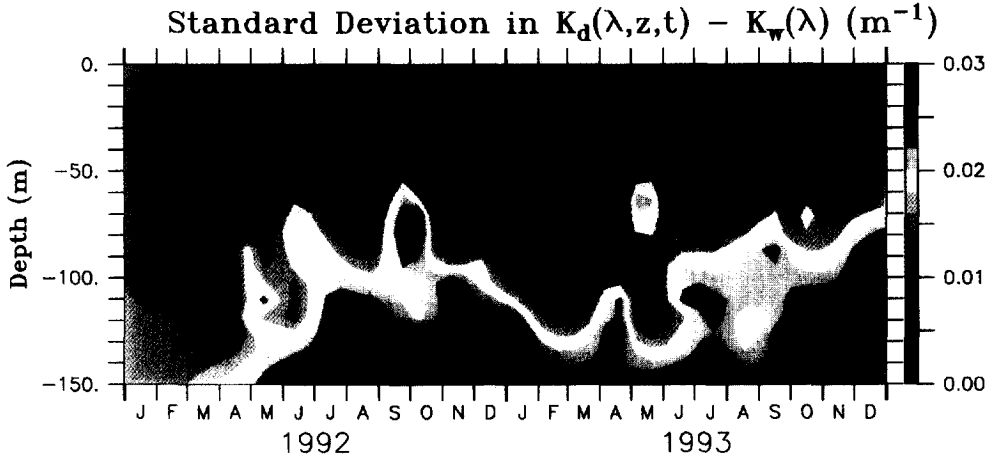


(a)

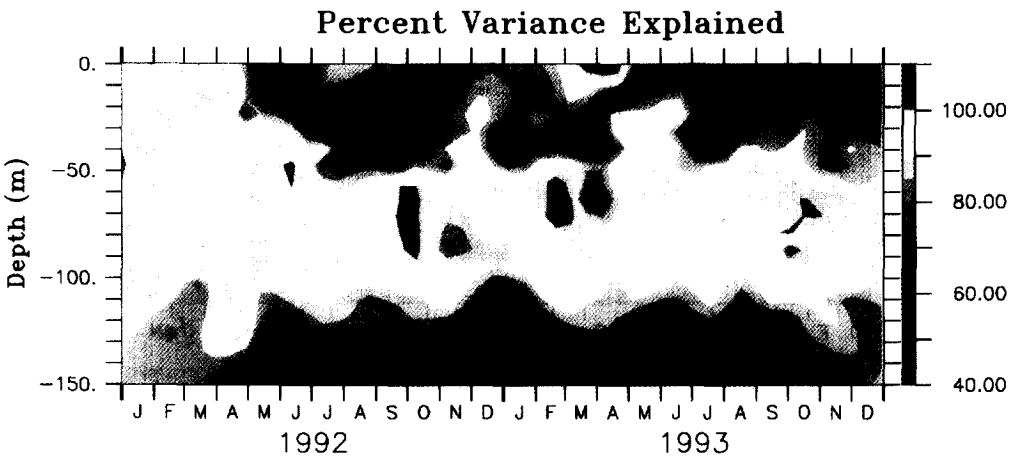


(b)

Fig. 5. Results from the spectral regression analysis for (a)  $K_{chl}(z, t, 440)$ , (b)  $K_{cdm}(z, t, 440)$  (above), (c) the root mean square difference between  $K_d(z, t, \lambda)$  and  $K_n(\lambda)$  (RMSD), and (d) the percentage RMSD predicted (next page). The "best" choice of model parameters are used (SB81, B95 and  $S = 0.014 \text{ nm}^{-1}$ ). Values of  $K_{chl}(z, t, 440)$ ,  $K_{cdm}(z, t, 440)$ , and RMSD are in units of  $m^{-1}$ .



(c)



(d)

Fig. 5. (c) and (d)

caused by inelastic scattering processes, such as Raman scattering and/or CDOM fluorescence, both of which will make  $K_d(z,t,565)$  behave similarly to the attenuation coefficients for the blue-green wavebands (e.g. Siegel and Dickey, 1987a; Stavn and Weidemann, 1992; Marshall and Smith, 1990). It is unlikely that the drop-off in  $K_d(z,t,565)$  values with depth is due to instrumental sources, such as light leakage in the  $E_d(z,t,565)$  sensor. This is because typical ratios of  $E_d(100\text{ m},t,565)$  to  $E_d(100\text{ m},t,441)$  are roughly 1:300, which is far greater than the 1:10<sup>6</sup> out-of-band rejection rate reported for three cavity interference filter photodetectors (Siegel *et al.*, 1986).

The extremely low, near-surface  $K_d(z,t,\lambda)$  values provide an excellent opportunity to re-evaluate estimates of the pure seawater attenuation spectrum  $K_w(\lambda)$  (Smith and Baker, 1981, hereafter SB81). SB81 compiled upper ocean mean determinations of  $K_d(\lambda)$  observations from many clear natural waters, including the Sargasso Sea, to estimate a minimum  $K_d(\lambda)$  spectrum. This minimum spectrum they referred to as the "pure seawater" diffuse attenuation coefficient spectrum, or  $K_w(\lambda)$ . It has recently been speculated that the SB81  $K_w(\lambda)$  spectrum may be contaminated by colored organic materials, particularly in the ultraviolet region of the spectrum (Kirk, 1994b). Evaluation of the smallest observed  $K_d(z,t,\lambda)$  values from the BBOP data set may provide an important, independent check on the SB81  $K_w(\lambda)$  determinations.

The observed  $K_d(z,t,\lambda)$  probability distributions range from  $> 0.01$  to  $< 0.1\text{ m}^{-1}$  for the 6 wavebands evaluated (Fig. 2). All valid  $K_d(z,t,\lambda)$  determinations were used in constructing these distributions ( $N = 1053$ ). The 1% percentile points of the probability density distributions ( $K_{\min}(\lambda)$ ; shown as the solid vertical lines in Fig. 2) are similar, although a bit lower, than the SB81 values (the dashed vertical lines in Fig. 2). This difference between our  $K_{\min}(\lambda)$  and the SB81  $K_w(\lambda)$  spectra increases with increasing wavelength (see also Fig. 3). This result is the same if data from only the upper 30 m of the water column are considered (not shown). This trend also may be found by evaluating the fraction of the observations where  $K_d(z,t,\lambda)$  values are less than the SB81  $K_w(\lambda)$  for both the entire data set and just the upper 30 m alone (Table 1). These findings suggest that inelastic scattering processes (i.e. Raman scatter, CDOM fluorescence, etc.) are important for producing the observed low values of  $K_{\min}(\lambda)$  for the higher wavelengths ( $\lambda \geq 520\text{ nm}$ ). Further, the difference between these two estimates of clear water attenuation implies that the SB81  $K_w(\lambda)$  spectrum is not contaminated with CDOM, at least compared with the present data (cf. Kirk, 1994b). Thus, the SB81 clear-water attenuation compilation remains an effective estimate for  $K_w(\lambda)$ .

Hints of the source(s) of  $K_d(z,t,\lambda)$  variability may be diagnosed by comparing values of  $K_d(z_o,t,\lambda)$  with the value of  $K_d(z_o,t,488)$  at a fixed depth  $z_o$ . This representation will accentuate relative changes in the blue portion of the  $K_d(z_o,t,\lambda)$  spectrum (Siegel *et al.*, 1995a). Within the mixed layer ( $z_o = 20\text{ m}$ ), the normalized  $K_d(20,t,\lambda)$  spectrum ( $= K_d(z_o,t,\lambda)/K_d(z_o,t,488)$ ) shows a strong seasonal cycle for the blue region of the spectrum ( $400 < \lambda < 450\text{ nm}$ ) (Fig. 4(a)). There, the normalized  $K_d(20,t,\lambda)$  increases smoothly with decreasing wavelength during the fall-to-spring seasons; while during the summers, few significant spectral variations are found. During the winter, the value of  $K_d(20,t,410)$  is 40% greater than  $K_d(20,t,488)$  (Fig. 4(a)). The winter-time spectral signature shows a rapidly increasing signal with decreasing wavelength indicative of colored dissolved organic and/or detrital particulate materials (equation (2)). This suggests that the winter mixed layer is characterized by relatively high CDM concentrations while the summer-time mixed layer should have very low or non-existent CDM concentrations. The normalized  $K_d(80,t,\lambda)$  spectrum also has a seasonal cycle, but it is temporally out of phase with the observations at

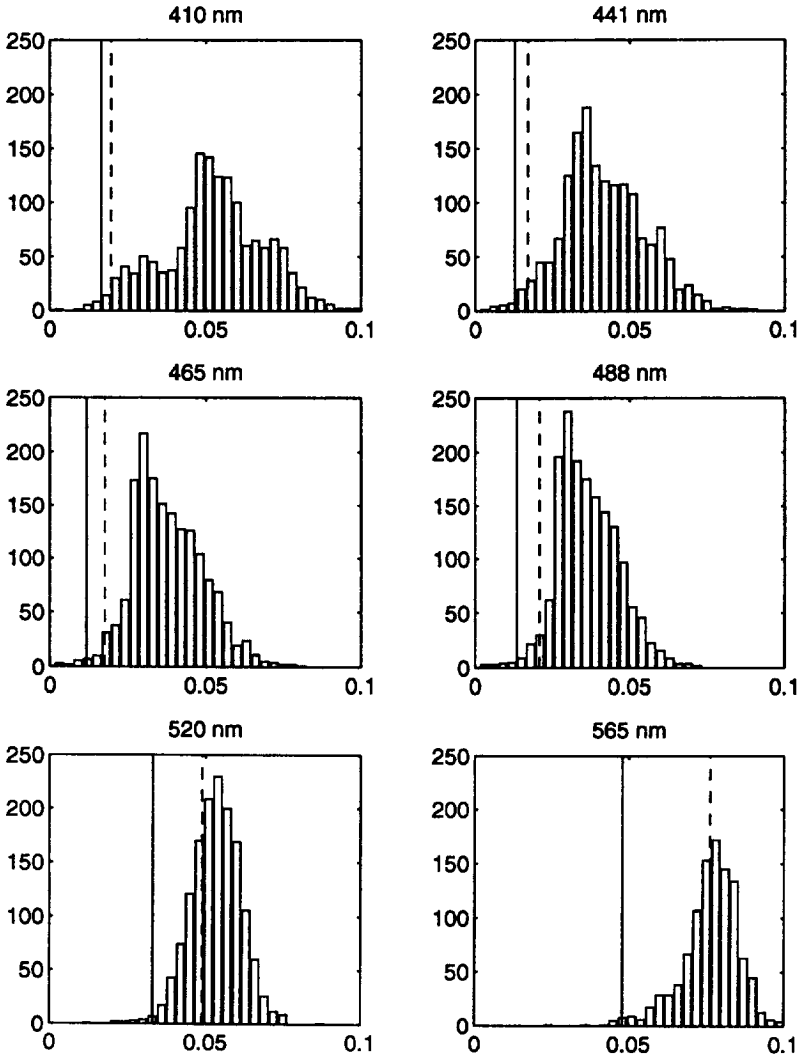


Fig. 2. Probability distributions for  $K_d(z, t, \lambda)$  where  $\lambda$  is equal to 410, 441, 465, 488, 520 and 565 nm. Determinations of  $K_d(z, t, \lambda)$  are in units of  $\text{m}^{-1}$ . A total of 1053 valid spectra are used in these distributions. The 1% percentile points of the probability density distribution ( $K_{\min}(\lambda)$ ) are shown as the vertical solid line and the SB81  $K_w(\lambda)$  values are indicated as the vertical dashed line in each of the probability distributions.

20 m (Fig. 4(b)). For  $\lambda < 450$  nm, values of normalized  $K_d(80, t, \lambda)$  increase during the summer and decrease in the winter. This suggests that CDM is produced at depth during the summer. Further, comparing the time-spectral patterns for the normalized  $K_d(20, t, \lambda)$  and  $K_d(80, t, \lambda)$  distributions indicates that there is, in general, more CDM at depth (80 m) than within the mixed layer.

Following Siegel *et al.* (1995a), a qualitative description of the time-depth evolution of CDM may be made by examining the ratio of  $K_d(z, t, 410)$  to  $K_d(z, t, 488)$  where elevated values of this ratio may be attributed to high CDM concentrations (Fig. 1(f)). The

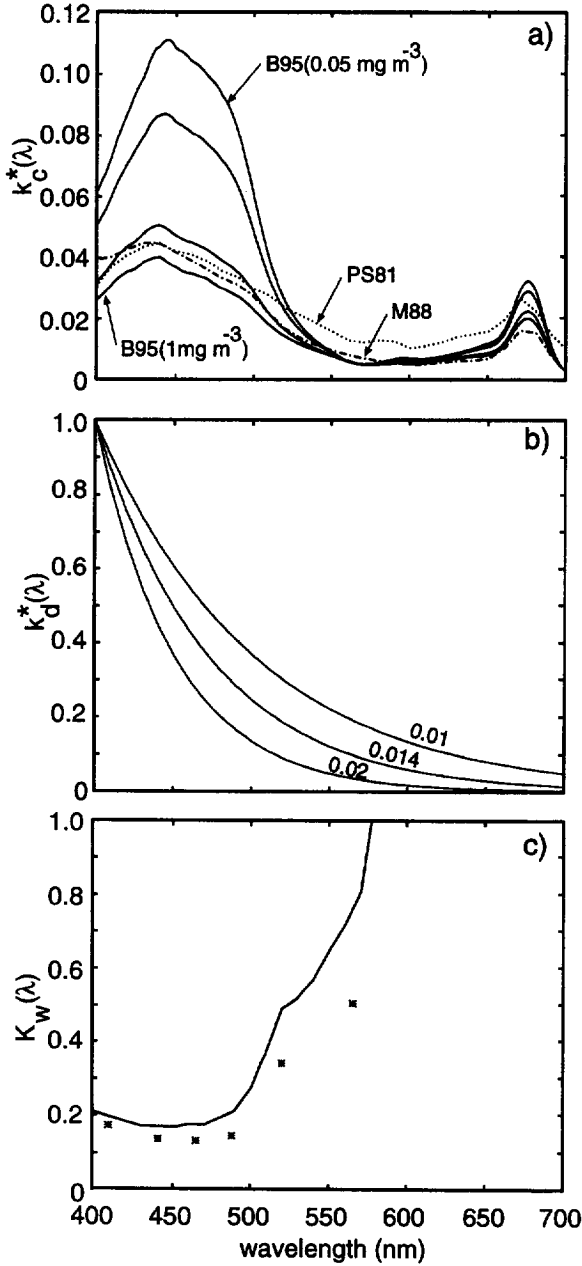


Fig. 3. Shapes used in the spectral regression analysis for (a) algal materials  $k_c^*(\lambda)$ , (b) colored dissolved materials  $k_d^*(\lambda)$  and (c) pure seawater  $K_w(\lambda)$ . For the  $k_c^*(\lambda)$  spectra (a), the  $a_{ph}^*(\lambda)$  spectrum is used and the spectra are in units of  $\text{m}^2 \text{mg}^{-1}$ . These spectra include the M88 compilation (dash-dot), the PS81 observed spectrum (dotted line, scaled to match the M88 spectrum at 440 nm) and the B95 in-vivo parameterization (the 4 solid lines). Chlorophyll  $a$  concentrations of 0.05, 0.1, 0.5 and 1  $\text{mg chl m}^{-3}$  are shown (top to bottom). For the  $k_d^*(\lambda)$  spectra (b), the exponential model is used (equation (2)) and slope parameter  $S$  of 0.01, 0.014 and 0.02  $\text{nm}^{-1}$  are shown from top to bottom. In (c), the SB81  $K_w(\lambda)$  spectrum is compared with the 1% percentile points of the  $K_d(z, t, \lambda)$  probability density distributions (\*s).

Table 1. Fraction of the  $K_d(z,t,\lambda)$  observations less than the SB81  $K_w(\lambda)$ 

$\lambda$	$K_w(\lambda)$	Per cent ( $z = \text{all}$ )	Per cent ( $z < 30 \text{ m}$ )
410	0.0196	2.6	12.3
441	0.0170	3.7	16.0
465	0.0176	3.3	13.7
488	0.0212	5.6	22.8
520	0.0489	13.9	37.9
565	0.0762	42.5	36.1

The column "Per cent ( $z = \text{all}$ )" refers to the percentage of observations where  $K_d(z,t,\lambda) < K_w(\lambda)$  for all depths whereas the "Per cent ( $z < 30 \text{ m}$ )" column refers to the percentage of observations where  $K_d(z,t,\lambda) < K_w(\lambda)$  only when  $z < 30 \text{ m}$ . The total number of 5 m subsampled  $K_d(z,t,\lambda)$  observations is equal to 1053 while only 219 are found at or above 30 m. The SB81 estimate of  $K_w(\lambda)$  is used.

superimposed red line in Fig. 1(f) indicates the time history of the mixed layer depth. The ratio of  $K_d(z,t,410)$  to  $K_d(z,t,488)$  illustrates significant seasonal variations in the mixed layer, where relatively high values ( $\sim 1.3$ ) are found during the fall and winter while lower values,  $\sim 1$ , are observed in the summer. At depth ( $> 70 \text{ m}$ ), this ratio of attenuation coefficients is relatively high ( $> 1.3$ ) throughout the year, although values are significantly higher in the summer months. This ratio does not decrease with depth below either the mixed layer depth or the subsurface chl *a* maximum (Fig. 1(e)). Using these data, a qualitative description of the CDM seasonal cycle may be made. Starting in the fall, high CDM waters at depth ( $\sim 80 \text{ m}$ ) are mixed into the upper layers and the CDM profile is homogenized. After spring-time stratification (March–May), CDM concentrations decrease within the upper mixed layer reaching a minimum in August–September. This reduction in mixed layer CDM concentration is probably due to photo-oxidation of CDM as mixed layer depths are rather shallow at this time (20–30 m) (e.g. Bricaud *et al.*, 1981; Nelson and Robertson, 1993). Below the summer mixed layer, the concentration of CDM increases significantly suggesting that CDM is produced at depth. Each fall this process repeats itself.

The role of CDM in spectral irradiance attenuation variability may be quantified by performing a two component regression analysis where we assume that variations in  $K_d(\lambda)$  are caused only by changes in the concentration of chlorophyll and CDM, or

$$K_d(z, t, \lambda) \cong K_w(\lambda) + \text{chl}(z, t)k_c^*(\lambda) + \text{CDM}(z, t)k_d^*(\lambda) \quad (3)$$

where  $k_c^*(\lambda)$  and  $k_d^*(\lambda)$  are the chlorophyll and CDM-specific attenuation coefficients, respectively. By assuming characteristic  $k_c^*(\lambda)$  and  $k_d^*(\lambda)$  spectral shapes, here taken from the literature (see below), estimates of CDM and chl can be made by over-constraining equation (3) with respect to wavelength. This will provide a "K-like" coefficient for CDM,  $K_{\text{cdm}}(z,t,\lambda)$  ( $= \text{CDM}(z,t) k_d^*(\lambda)$ ), and a similar coefficient for chlorophyll,  $K_{\text{chl}}(z,t,\lambda)$  ( $= \text{chl}(z,t) k_c^*(\lambda)$ ). These parameters provide quantitative estimates of the role of colored detrital and algal materials on  $K_d(z,t,\lambda)$  variations. Calculations are made over the upper 150 m and only wavelengths less than 565 nm (inclusively) are used in order to minimize the effects of Raman scattering and CDOM fluorescence. Also, the spectral regression is performed only if the root mean squared difference between the observed value of  $K_d(z,t,\lambda)$  and the  $K_w(\lambda)$  estimate (summed over the six wavebands employed) is greater than

$0.005 \text{ m}^{-1}$  (where the SB81  $K_w(\lambda)$  estimate is used; Fig. 5(c)). If values of this root mean square deviation (RMSD) are found to be less than  $0.005 \text{ m}^{-1}$ , the retrieved values of  $\text{CDM}(z,t)$  and  $\text{chl}(z,t)$  are set equal to zero.

The proper choices of characteristic shapes for the  $k_c^*(\lambda)$  and  $k_d^*(\lambda)$  spectra, as well as the correct specification of  $K_w(\lambda)$ , are critical for the realistic application of equation (3) for determining CDM and algal attenuation coefficients. Here, we assume that  $k_c^*(\lambda)$  and  $k_d^*(\lambda)$  can be modeled using their respective specific absorption coefficients ( $a_{ph}^*(\lambda)$  and  $a_d^*(\lambda)$ ) and that the  $K_w(\lambda)$  spectrum is known. In order to determine the "best" choice of model parameters, we perform a sensitivity analysis comparing reasonable candidate models. For example, the degree of success of using three different formulations for  $k_c^*(\lambda)$  are evaluated using previously determined estimates of  $a_{ph}^*(\lambda)$  (Morel, 1988 [M88]; Prieur and Sathyendranath, 1981, [PS81]; Bricaud *et al.*, 1995 [B95]; Fig. 3(a)). The M88 spectrum is based upon a compilation of laboratory culture data (14 species in total) whereas the PS81 spectrum was determined through a statistical analysis of in-situ absorption spectra and the B95 spectrum is based upon a global data set of in-vivo  $a_{ph}^*(\lambda)$  spectra. In particular, the shape of the B95  $a_{ph}^*(\lambda)$  spectrum is dependent upon the chl *a* concentration in order to model the effects of photoadaptation and the pigment packaging effect (Kirk, 1994a; Nelson *et al.*, 1993; B95) whereas the shapes of the M88 and PS81  $a_{ph}^*(\lambda)$  spectra are constant. The shape of the B95  $a_{ph}^*(\lambda)$  spectral distributions are similar to the M88 and PS81 models only for relatively high ( $\geq 1 \text{ mg m}^{-3}$ ) chl *a* concentrations (Fig. 3(a)). This indicates that the M88 and PS81  $a_{ph}^*(\lambda)$  spectra correspond to high chlorophyll environments and hence, may not be truly effective for modeling algal optical properties in relatively clear open ocean waters (see also Garver and Siegel, submitted). As with the chlorophyll-specific attenuation coefficient, the CDM attenuation was modeled using its absorption coefficient (equation (2)) and a range of exponential slope parameter values were used ( $S = 0.010, 0.014$  and  $0.020 \text{ nm}^{-1}$ ; Fig. 3(b)).

In order to determine the "best" combination of optical model shapes, a sensitivity analysis was performed by applying each permutation of model shapes to the regression model (equation (3)) over the entire data set. The "best" model was determined by assessing the fraction of the total number of independent  $K_d(z,t,\lambda)$  spectra which explain more than 50, 80 and 90% of the variance in  $K_d(z,t,\lambda)$  (Table 2). Regression analyses using the B95  $a_{ph}^*(\lambda)$  spectrum required nonlinear numerical optimization techniques to be employed (the quasi-Newton method) as opposed to linear least squares. It is apparent that the "best" model is comprised of the B95  $a_{ph}^*(\lambda)$  shape, an  $S$  value of  $0.014 \text{ nm}^{-1}$  and the SB81  $K_w(\lambda)$  spectrum (Table 2). This model explains more than 90% of the variance for over 70% of the valid observations. This is far better than any of the other regression model formulations, which typically explain more than 90% of the variance in  $K_d(z,t,\lambda)$  for less than about 55% of the data set (Table 2). Changes in the  $k_c^*(\lambda)$  shape appeared to have less influence on the "success" of the retrievals than did the selected value of the CDM exponential slope parameter  $S$ . The final value of  $0.014 \text{ nm}^{-1}$  is characteristic of many marine systems (Carder *et al.*, 1989; Roesler *et al.*, 1989; Nelson and Robertson, 1993; Kirk, 1994a). In addition, the use of  $K_{\min}(\lambda)$  (Fig. 3(c)) as an estimate of  $K_w(\lambda)$  in the regression model results in very poor regression coefficients (Table 2).

In general, values of  $K_{\text{cdm}}(z,t,440)$  are nearly as large as  $K_{\text{chl}}(z,t,440)$ , indicating that colored detrital and dissolved materials make nearly an equal contribution to the in-situ  $K_d(z,t,\lambda)$  as the attenuation due to algal pigments (Fig. 5(a) and 5(b)). In particular, the  $K_{\text{cdm}}(z,t,440)$  distribution (Fig. 5(b)) exhibits the same basic time-depth pattern as our

Table 2. Sensitivity analysis of regression model parameters

$K_w(\lambda)$	$k_c^*(\lambda)$	$S$ (nm <sup>-1</sup> )	Percentage > 50%	Percentage > 80%	Percentage > 90%
SB81	B95	0.014	94	84	70
SB81	B95	0.010	94	69	33
SB81	B95	0.020	92	81	54
SB81	M88	0.014	88	73	57
SB81	M88	0.010	87	68	44
SB81	M88	0.020	88	76	61
SB81	PS81	0.014	88	73	53
SB81	PS81	0.010	87	66	42
SB81	PS81	0.020	89	75	56
$K_{\min}(\lambda)$	M88	0.014	19	11	6
$K_{\min}(\lambda)$	M88	0.010	25	15	9
$K_{\min}(\lambda)$	M88	0.020	18	9	5

Percentage retrievals with variance explained greater than 50, 80 and 90% are provided for the different regression models. The total number of  $K_d(z,t,\lambda)$  observations used is 1053. SB81 refers to the Smith and Baker (1981) estimate of  $K_w(\lambda)$ ,  $K_{\min}(\lambda)$  utilizes the presently derived estimate for  $K_w(\lambda)$ , M88 refers to the Morel (1988)  $a_{ph}^*(\lambda)$  shape, PS81 employs the Prieur and Sathyendranth (1981)  $a_{ph}^*(\lambda)$  shape, and B95 uses the Bricaud *et al.* (1995)  $a_{ph}^*(\lambda,chl-a)$  function.

qualitative indicator of CDM attenuation diagnosed using the ratio of  $K_d(z,t,\lambda)$  to  $K_d(z,t,\lambda)$  (Fig. 1(f)). This supports the use of this ratio as a qualitative indicator of CDM concentrations (Siegel *et al.*, 1995a). The highest values of CDM ( $\sim 0.03$  m<sup>-1</sup>) are found below the summer-time mixed layer. This is consistent with the hypothesis that CDM is produced within the summer pycnocline (for depths  $\geq 80$  m). The lowest values of  $K_{cdm}(z,t,440)$  are found in the summer-time mixed layer. This again is consistent with our hypothesis that this material is photo-bleached during the summer due to the high light dosage received in the shallow (20–30 m) summer mixed layer (Fig. 1(f)). The time–depth distribution of  $K_{chl}(z,t,440)$  exhibits elevated values within the deep chlorophyll maximum and during the bloom periods, similar to the chl *a* concentration (Fig. 1(e)). However, the depiction of algal light attenuation coefficient is much noisier than that for  $K_{cdm}(z,t,440)$  (Fig. 5(a) and 5(b)).

The spectral variability in  $K_d(z,t,\lambda)$  to be explained by the regression analysis is given by the distribution of the root mean squared deviation (RMSD) between  $K_d(z,t,\lambda)$  and the SB81 determination of  $K_w(\lambda)$  (summed over the six wavebands used; Fig. 5(c)). Values of RMSD are at their highest in the sub-surface chl *a* maximum and when surface chl *a* concentrations are elevated, as expected. Values of RMSD are also high for depths greater than 100 m. This is probably due to large differences between  $K_d(z,t,\lambda)$  and  $K_w(565)$  caused by either CDOM fluorescence and/or Raman scattering. The percentage of the RMSD explained by the spectral regression model generally has its highest values where RMSD values are large (Fig. 5(d)) and for depths less than  $\sim 100$  m. This is particularly true within the depth range where subsurface chl *a* concentrations are elevated (roughly between 40 and 110 m; Figs 1(e) and 5(d)). The percentage of the variance explained is low within the near-surface mixed layer during the summer. These waters appear to contain little optically relevant particulate or dissolved materials. The percentage of the variance explained by the model is also low below the sub-surface chl *a* maximum where nonlinear scattering processes are active.

## DISCUSSION

We have shown that a significant fraction of the spectral light attenuation in the Sargasso Sea is regulated by materials other than chlorophyll pigment concentrations. The relatively large fraction of the total amount of spectral diffuse attenuation that is regulated by these colored detrital materials (CDM) is fairly startling. Here, we have characterized CDM concentrations using in-situ optical data. Hence, we do not know whether CDM is dissolved or particulate or both. The resolution of this question is critical if we are to understand what regulates its variability. Further, we do not understand the role that CDM plays in biogeochemical cycling of materials in the upper ocean nor how it affects our attempts to determine algal properties from an ocean color signal. Below, we discuss several of these issues and suggest the next steps towards resolving these questions.

### *What is CDM?*

The regression analysis performed in the previous section extracted a component of the diffuse attenuation coefficient spectrum,  $K_d(z, t, \lambda)$ , with an exponentially decaying spectrum with exponential slope equal to  $0.014 \text{ nm}^{-1}$ . By relating this retrieved component with previously published spectra for detrital particulate and colored organic dissolved materials, we referred to this signal ( $K_{\text{cdm}}(z, t, \lambda)$ ) as the colored detrital material, or CDM, concentration. But, what is CDM, what are its properties and what regulates its variability? The answers to these questions are critical if we are to understand its role in upper ocean biogeochemical cycling.

There are several quantities measured at BATS that can be compared to the observed patterns of CDM variability. Among these properties are dissolved organic carbon (DOC) and particulate organic carbon (POC) concentrations. Close matches in the time–depth patterns of DOC or POC would suggest that these operationally defined pools of carbon are related to the composition of CDM, while strong mismatches will indicate that either DOC or POC does not contribute significantly to CDM.

Seasonal mean vertical profiles of  $K_{\text{cdm}}(440)$  and DOC (DOC data from Carlson *et al.*, 1994) show no apparent correlation with one another, with the exception of the winter when deep mixing homogenizes both signals with depth (Fig. 6(a) and 6(b)). In particular, CDM estimates are low (near zero) in the summer-time mixed layer when the DOC values are relatively high (compared to the vertically uniform winter-time value). Surface DOC declines steadily throughout the spring, summer and fall, while CDM decreases rapidly to a mid-summer minimum and then increases in the fall. Below 80 m, DOC concentrations are relatively low and decline through the year due to remineralization, while the CDM estimates remain high throughout the summer (Figs 6(a), 6(b) and 5(b)). Thus, the CDM estimates are not directly related to the DOC concentration. This means that if CDM is comprised of dissolved organic materials, it only represents a small fraction of the total amount of DOC. Further, the observed CDM variations do not covary with the DOC, which will make the estimation of DOC from an optical measure of CDM difficult at best.

The concentration of particulate organic carbon (POC) quantifies the total amount of carbon found within particulate materials, some of which will be detrital. Although there is considerable scatter, seasonal vertical profiles of POC concentration show little relationship with the CDM estimates (Fig. 6(c)). Hence, POC is also a poor predictor of CDM concentrations. Phaeopigment concentrations estimated by fluorometry, after correction

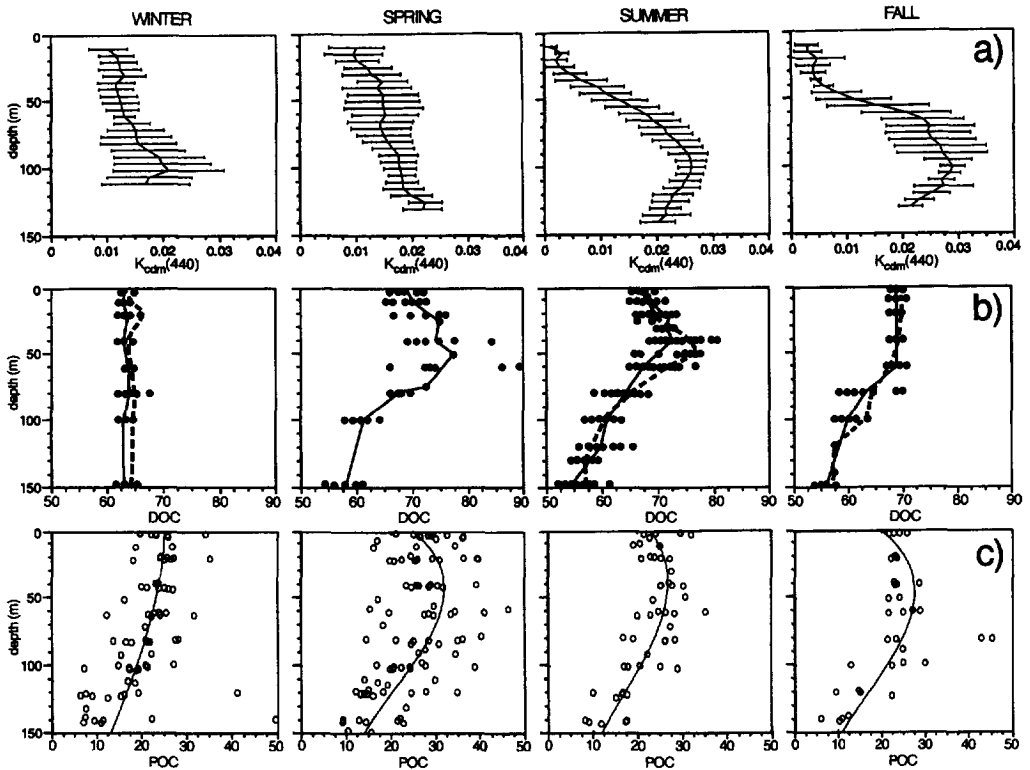


Fig. 6. Seasonal vertical profiles of (a) CDM attenuation ( $K_{\text{cdm}}(440)$  in units of  $\text{m}^{-1}$ ), (b) dissolved organic carbon (DOC in units of  $\mu\text{mol l}^{-1}$ ), and (c) particulate organic carbon (POC in units of  $\mu\text{g kg}^{-1}$ ) for each of the four seasons of 1992 and 1993. The data are aggregated into the spring (March-April-May), summer (June-July-August), fall (September-October-November) and winter (December-January-February) seasons. The error bars in (a) represent the standard deviation envelope while in (c) the lines represent polynomial best-fits. The DOC data are redrafted from Carlson *et al.* (1994) and the differing lines represent mean profiles for different years (solid = 1992 and dashed = 1993).

for the presence of chl *b* and *c* (Vernet and Lorenzen, 1987), are not significantly different from zero for any of the present data set. Hence, phaeopigment concentrations are of little relevance for assessing the source of CDM. A similar lack of correspondence is observed between CDM attenuation and bacterioplankton abundances (not shown).

Obviously, we can not answer the question of what comprises CDM from the simple bulk material distributions provided from the existing BATS data set. The observed temporal and depth variations in CDM simply do not look like either DOC or POC, our best indicators for dissolved organic materials and detrital particulates. Colored detrital materials are an important optical signal that is not sampled by any of the standard biogeochemical measurements made at BATS. Although we cannot conclude that CDM is comprised of either dissolved organic or detrital particulate materials, it is apparent that CDM must be comprised of a small fraction of the total DOC or POC in the water column. It is possible that CDM reflects a more labile fraction of the total DOC or POC pools and that CDM may be a useful indicator for this important quantity. However, it is just as likely

that CDM is just one of many labile components that comprise the combined pools of DOC and POC. It is clear that neither DOC nor POC can be estimated by an optical estimate of CDM. The elucidation of the materials that comprise CDM and its role in biogeochemical material cycling remains a focus of on-going work at BBOP and BATS.

### *Implications for ocean biogeochemistry*

The time–depth pattern of the CDM light attenuation coefficient provides several important clues to its creation and destruction and some hints of its role in ocean biogeochemistry (Fig. 5(b)). First, CDM appears to be produced and destroyed locally. This means that these non-algal colored materials are definitely not of terrestrial origin, as is often speculated (e.g. Jerlov, 1976; Walsh *et al.*, 1992; Zika *et al.*, 1993; Kirk, 1994a). Second, as CDM concentrations vary on the same timescales as the seasonal patterns of upper ocean biogeochemical cycling, it must be comprised of labile materials that are readily produced and destroyed on this timescale.

A third biogeochemically relevant implication of the observed CDM variability is its link to upper ocean photochemistry. Many photochemical reactions are driven by photons absorbed by dissolved organic materials (e.g. Zika *et al.*, 1993; Sikorski and Zika, 1993; Weiss *et al.*, 1995). The absorbed photochemically usable radiation (PCUR) can be expressed as

$$\text{PCUR}(z, t) = \int_{\lambda_{\text{solar}}} \frac{\lambda}{hc} a_{\text{pcur}}(\lambda) E_o(z, t, \lambda) d\lambda \quad (4)$$

where  $a_{\text{pcur}}(\lambda)$  is the absorption coefficient for the photochemically relevant materials,  $E_o(z, t, \lambda)$  is the scalar irradiance spectrum,  $hc = 1.99 \times 10^{-16}$  J nm quanta<sup>-1</sup>, and  $\lambda_{\text{solar}}$  represents integration over the entire solar spectrum. The term  $\lambda/hc$  converts from energy to quanta (or photon) units. The PCUR flux quantifies the potential for photochemical work; how that absorbed radiation is utilized to perform photochemistry is another story (using the relevant quantum yield). It is apparent from an examination of equation (4) that the potential for photochemical reactions will be modulated by the intensity of the in-situ irradiance spectrum, the absorption properties of the photochemically relevant materials in the water column, and probably to a lesser extent by the spectral quality of the in-situ irradiance (Siegel *et al.*, 1995a). Values of PCUR will be high when CDM values are elevated (related to  $a_{\text{pcur}}(\lambda)$ ), and when the in-situ irradiance spectral intensity is high (related to the incident flux of photosynthetically available radiation, PAR). The product of two factors describe the relative potential for photochemical work.

The photochemical potential can be evaluated using the time evolution of upper ocean mean CDM estimates and the daily mean flux of PAR just beneath the sea surface,  $\overline{\text{PAR}}(0^-)$  (Fig. 7(a) and 7(b)). The error bars for the CDM distribution quantify the variability (standard deviation) in CDM estimates for the upper 30 m (Fig. 7(a)). Attenuation coefficients for CDM at 440 nm demonstrate the large seasonal cycle commented upon previously where upper ocean estimates vary from near-zero during the summer to  $\sim 0.015 \text{ m}^{-1}$  in the winter periods of deep mixing (Fig. 7(a)). Values of  $\overline{\text{PAR}}(0^-)$  are determined only for those days where the in-situ primary production array is deployed (29 out of 731 possible days during 1992 and 1993; Siegel *et al.*, 1995a). Hence, these estimates do not provide adequate resolution of the long-term light dosage relevant for

evaluating the potential for photochemical work. The daily integrated PAR flux,  $\overline{\text{PAR}}(0^-)$ , also illustrates a seasonal pattern with the higher fluxes in the summer. The amplitude of the  $\overline{\text{PAR}}(0^-)$  seasonal cycle is a factor of nearly three. However, there is strong variability in  $\overline{\text{PAR}}(0^-)$  associated with extreme, short timescale changes in cloud abundance, particularly for the summer months (Fig. 7(b)). The magnitude of these cloud-induced changes in  $\overline{\text{PAR}}(0^-)$  is at least as large as seasonal changes due to the Earth's planetary cycles. In order to best evaluate the role of long-term light dosage on upper layer photochemistry, we apply a clear-sky solar radiation model (Seckel and Beaudry (1973), scaled to match the peak-to-peak amplitudes of the  $\overline{\text{PAR}}(0^-)$  determinations) to estimate relative time variations in PCUR (Fig. 7(b)). The product of CDM and the modeled PAR flux provides an estimate of the relative PCUR flux,  $\text{PCUR}_{\text{rel}}$ , for the mixed layer (Fig. 7(c)). Values of  $\text{PCUR}_{\text{rel}}$  are scaled so that its maximum value is equal to one. Time variations of  $\text{PCUR}_{\text{rel}}$  show a significant seasonal cycle, similar to that observed for CDM, where the smallest values are

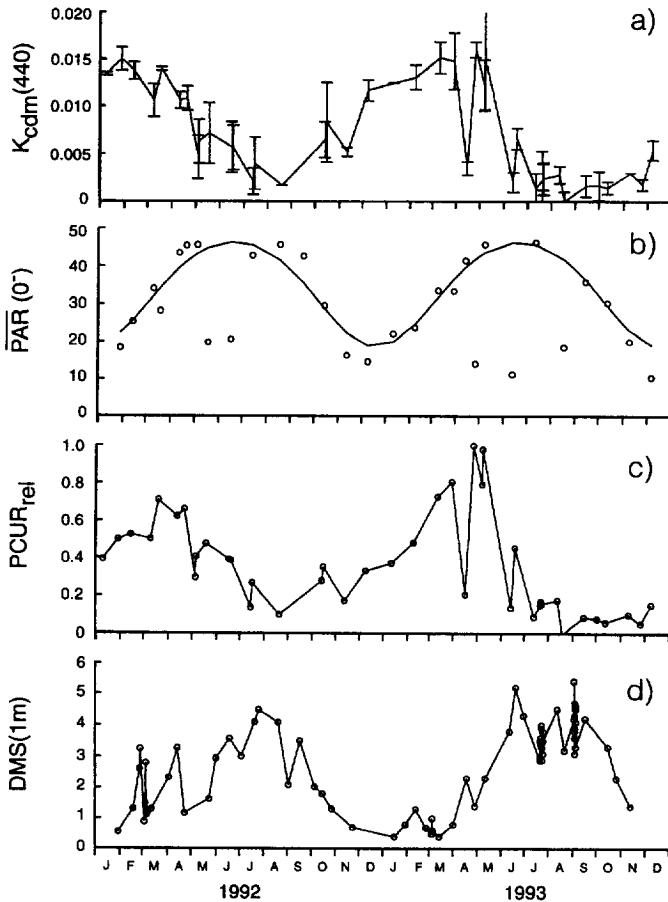


Fig. 7. Time history of (a) upper 30 m mean  $K_{\text{cdm}}(440)$  (in units of  $\text{m}^{-1}$ ), (b) the incident PAR flux ( $\overline{\text{PAR}}(0^-)$ ) with the scaled clear-sky flux (in  $\text{Einstein m}^{-2} \text{ day}^{-1}$ ), (c) relative variations in the photochemically usable radiation ( $\text{PCUR}_{\text{rel}}$ ; no units), and (d) upper bottle (1 m) dimethyl sulfide concentration (in  $\text{ng l}^{-1}$ ). The error bars in (a) represent the standard deviation envelope.

found in the summer months (Fig. 7(c)). Hence, we would expect that the potential for photochemical reactions will be at a minimum during the summer and that those materials which are produced (or destroyed) by photochemical reactions may be at a seasonal minimum (maximum) during this time.

We explore this prediction by comparing  $PCUR_{rel}$  with the seasonal evolution of dimethyl sulfide (DMS) concentrations measured simultaneously at BATS (Dacey *et al.*, submitted). Dimethyl sulfide is a trace gas produced within the marine environment, which may play an important role in the radiative balance of the atmosphere (cf. Charlson *et al.*, 1987; Falkowski *et al.*, 1992). DMS is produced from dimethyl sulfoniopropionate (DMSP) through bacterial cleavage of dissolved DMSP and by metazoan grazing of algal species which contain DMSP. Mixed layer DMS in turn, is lost by a combination of biological oxidation by bacteria, air-sea fluxes and photochemical oxidation (e.g. Dacey and Wakeham, 1986; Brimblecombe and Shooter, 1986; Malin *et al.*, 1992).

Concentrations of DMS within the mixed layer are highest in the summer and lowest in the winter (Fig. 7(d), see Dacey *et al.*, submitted, for more details). This summer maximum must arise from a combination of higher rates of DMS production and lower rates of loss compared to the rest of the year. Seasonal variations in the rate of conversion of DMSP to DMS are difficult to estimate, though DMSP concentrations are relatively high throughout the spring-fall period (Dacey *et al.*, submitted). Losses by gas exchange should be higher during the summer since the increase in DMS concentration is significantly more important to the air-sea gas flux than is the coincident decline in wind speeds. Biological oxidation of DMS seems slow throughout the year at BATS (Dacey *et al.*, submitted). A summer minimum in photo-oxidation would contribute significantly to the observed patterns in DMS. We hypothesize that the seasonal cycle in DMS is, at least partially, due to a reduction in photo-oxidation rates caused by small relative values of CDM during the summer. This hypothesis is testable by coupling optical estimates of CDM with detailed investigations of the photo-oxidation of DMS in natural waters.

#### *Implications for remote sensing*

The present observations illustrate that CDM concentrations are an important component of the light attenuation budget. For remote sensing applications, CDM must be considered in retrieving chlorophyll concentrations from observations of ocean color even in the open ocean. The effect of CDM on ocean color spectra can be demonstrated by examining the effects of CDM on band-ratio chlorophyll algorithms (e.g. Gordon and Morel, 1983). Typically, upper layer chlorophyll pigment concentrations, CHL, are determined from ocean color spectra using the ratio of the remotely sensed reflectance at 441 and 565 nm ( $R_{rs}(441)$  and  $R_{rs}(565)$ ;  $R_{rs}(\lambda) = L_u(\lambda)/E_d(\lambda)$ ), or

$$CHL = A \left( \frac{R_{rs}(441)}{R_{rs}(565)} \right)^{-B} \quad (5)$$

where typical values for  $A$  and  $B$  are 1.23 and 1.7, respectively (e.g. Gordon and Morel, 1983). Detailed optical modeling has empirically linked  $R_{rs}(\lambda)$  determinations to the inherent optical properties of the upper ocean and thereby to apparent optical properties (Gordon *et al.*, 1988), or

$$R_{rs}(\lambda) \cong \text{const.} \frac{b_b(\lambda)}{a(\lambda)} \cong \text{const.} \frac{b_b(\lambda)}{K_d(\lambda)} \quad (6)$$

where  $a(\lambda)$  is the total absorption coefficient,  $b_b(\lambda)$  is the backscatter coefficient and the constants are, of course, different. The CHL band ratio algorithm (equation (5)) may be now expressed as

$$\text{CHL} \cong A \left( \frac{b_b(441) K_d(565)}{b_b(565) K_d(441)} \right)^{-B} \quad (7)$$

For the situation at BATS, we can assume that the backscattering coefficient will be due mostly to the water component (Morel and Gentili, 1991; Garver and Siegel, submitted). Further, the present measurements of  $K_d(565)$  are approximately constant within the upper 30 m with a mean value of  $\sim 0.08 \text{ m}^{-1}$  (Fig. 1(d)). Thus, CHL may be approximated as

$$\text{CHL} \cong A' K_d(441)^B \quad (8)$$

where  $A'$  lumps the assumed constant  $K_d(565)$  value and the backscattering coefficient ratio. The value of  $A'$  (15.9) is determined assuming that  $b_b(\lambda)$  may be expressed using its pure water value (SB81). Using this information, the effects of the band-ratio CHL estimate due to CDM concentrations can be estimated as

$$\Delta \text{CHL} \cong \frac{\partial \text{CHL}}{\partial K_{\text{cdm}}(441)} \Delta K_{\text{cdm}}(441) \cong A' B K_d(441)^{B-1} \Delta K_{\text{cdm}} \quad (9)$$

Thus, an increase  $K_{\text{cdm}}(441)$  will result in an overestimate of the CHL estimate. Assuming a typical winter  $K_d(441)$  value of  $0.03 \text{ m}^{-1}$  (Fig. 1(b)) and an observed mixed layer  $K_{\text{cdm}}(441)$  value of  $0.015 \text{ m}^{-1}$  (Fig. 7), the corresponding overestimate in CHL retrieval is  $\sim 0.024 \text{ mg m}^{-3}$ . Considering that typical early-winter chl  $a$  concentrations near the surface are  $\sim 0.04\text{--}0.06 \text{ mg m}^{-3}$  (Fig. 1(e)), the observed CDM light attenuation would be responsible for CHL overestimates of roughly 40–60%. This result is significant and indicates that the effects of colored non-algal materials must be explicitly assessed in the ocean color remote sensing algorithms (e.g. Carder *et al.*, 1986, 1989, 1991; Garver and Siegel, submitted).

As we have discussed previously, even if CDM attenuation is accounted for in the retrieval of near-surface chlorophyll concentrations, the resulting CDM estimate will not correspond to dissolved organic carbon concentrations, at least for this site. Thus, one must be very careful in assuming that colored detrital particulate and dissolved organic material optical properties are simply related to biogeochemically relevant properties.

### Implications for ocean optics

As we have shown, the spectral light attenuation budget within the clear Sargasso Sea is not a simple function of algal pigment concentration. It is likely that this is the case at other open ocean sites as this signal is detected only because of the consistent, long-term sampling conducted as part of the BATS program. Our observations of colored detrital particle and/or dissolved organic materials show significant time and space variations that do not covary with changes in chlorophyll concentrations. This is an important distinction for how the optical properties of ocean waters are characterized. For example, Case I waters are defined as those where “nothing besides algae, with their associated retinue, can influence the

optical properties" (p. 273, Morel, 1991). Case II waters are those waters where additional sources of light attenuation are important, generally of terrestrial origin (cf. sediments, CDOM, etc.). We show that for an architypal Case I water site, the Sargasso Sea, that detrital particulate and/or colored dissolved organic materials are a significant and variable fraction of the total light attenuation budget and that these colored materials do not covary with algal pigments concentrations. Strictly speaking, the BATS site more closely meets the definition of Case II waters. This is not to say that the optical properties of the Sargasso Sea are regulated by terrestrial processes, but rather that our simplistic characterizations of nature must be constantly re-examined.

*Acknowledgements*—The authors thank the field technicians involved in the BATS program for their dedication and commitment to the data presented here. In particular, the efforts of BBOP field technicians, Melodie Hammer and Liz Caporelli, are gratefully acknowledged. Margaret O'Brien performed the processing and maintenance of the BBOP data set. Erik Fields and John Ubante helped in the analysis and plotting of data set. Dave Menzies performed the quarterly calibrations of the BBOP radiometer and Julie Siegel provided editorial assistance. Discussions with Craig Carlson, John Dacey, Sara Garver, Norm Nelson, and Jens Sorensen, as well as comments from the reviewers, have been helpful. BBOP is supported by NASA, the SeaWiFS project office and NSF (OCE 91-16372 and OCE 90-16990). NSF also supports the core BATS program (OCE 88-01089, OCE 93-01950). The dimethyl sulfide time-series was supported by NSF grants to Drs John Dacey, Anthony Michaels and Stuart Wakeham (OCE 91-23419). This is contribution number 1412 from the Bermuda Biological Station for Research.

## REFERENCES

- Atlas D. and T. T. Bannister (1980) Dependence of mean spectral extinction coefficient of phytoplankton on depth, water color, and species. *Limnology and Oceanography*, **25**, 157-159.
- Baker K. S. and R. C. Smith (1980) Quasi-inherent characteristics of the diffuse attenuation coefficient for irradiance. *Proceedings of the Society of Photo-Optical Instrumentation Engineers, Ocean Optics VI*, **208**, 60-63.
- Baker K. S. and R. C. Smith (1982) Bio-optical classification and model in natural waters, II. *Limnology and Oceanography*, **27**, 500-509.
- Blizard M. A. (1986) Ocean optics: Introduction and overview. *Proceedings of the Society of Photo-Optical Instrumentation Engineers, Ocean Optics VIII*, **637**, 2-17.
- Blough N. V., O. C. Zafiriou and J. Bonilla (1993) Optical absorption spectra of waters from the Orinoco River outflow: Terrestrial input of colored organic matter to the Caribbean. *Journal of Geophysical Research*, **98**, 2271-2278.
- Bricaud A., A. Morel and L. Prieur (1981) Absorption by dissolved organic matter of the sea (yellow substance) in the UV and visible domains. *Limnology and Oceanography*, **26**, 43-53.
- Bricaud A., M. Babin, A. Morel and H. Claustre (1995) Variability in the chlorophyll-specific absorption coefficients of natural phytoplankton—analysis and parameterization. *Journal of Geophysical Research*, **100**, 13,321-13,332.
- Brimblecombe P. and D. Shooter (1986) Photo-oxidation of dimethylsulfide in aqueous solution. *Marine Chemistry*, **19**, 343-353.
- Carder K. L., R. G. Steward, J. H. Paul and G. A. Vargo (1986) Relationships between chlorophyll and ocean color constituents as they affect remote-sensing reflectance models. *Limnology and Oceanography*, **31**, 403-413.
- Carder K. L., R. G. Steward, G. R. Harvey and P. B. Ortner (1989) Marine humic and fulvic acids: Their effects on remote sensing of ocean chlorophyll. *Limnology and Oceanography*, **34**, 68-81.
- Carder K. L., S. K. Hawes, K. A. Baker, R. C. Smith, R. G. Steward and B. G. Mitchell (1991) Reflectance model for quantifying chlorophyll *a* in the presence of productivity degradation products. *Journal of Geophysical Research*, **96**, 20,599-20,611.
- Carlson C. A., H. W. Ducklow and A. F. Michaels (1994) Annual flux of dissolved organic carbon from the euphotic zone in the northwestern Sargasso Sea. *Nature*, **371**, 405-408.
- Charlson R. L., J. E. Lovelock, M. O. Andreae and S. E. Warren (1987) Oceanic phytoplankton, atmospheric sulfur, cloud albedo and climate. *Nature*, **326**, 655-661.

- Cleveland J. S. and M. J. Perry (1994) A model for partitioning particulate absorption into phytoplanktonic and detrital components. *Deep-Sea Research I*, **41**, 197–221.
- Dacey J. W. H. and S. G. Wakeham (1986) Oceanic dimethylsulfide: Production during zooplankton grazing on phytoplankton. *Science*, **233**, 1314–1316.
- Dacey J. W. H., F. Howse, A. F. Michaels and S. G. Wakeham (submitted) Temporal variability of DMS and DMSP in the Sargasso Sea. Submitted to *Deep-Sea Research*.
- Falkowski P. G., Y. Kim, Z. Kolber, C. Wilson, C. Wirick and R. Cess (1992) Natural versus anthropogenic factors affecting low-level cloud albedo over the North Atlantic. *Science*, **256**, 1311–1313.
- Garver S. and D. A. Siegel (submitted) Inherent optical property inversion of ocean color spectra and its biogeochemical interpretation: 1. Time-series from the Sargasso Sea. *Journal of Geophysical Research*.
- Garver S., D. A. Siegel and B. G. Mitchell (1994) A statistical analysis of particulate absorption spectra: What can a satellite ocean color imager see? *Limnology and Oceanography*, **39**, 1349–1367.
- Gordon H. R. (1989) Can the Lambert–Beer law be applied to the diffuse attenuation coefficient of ocean water? *Limnology and Oceanography*, **34**, 1389–1409.
- Gordon H. R. and A. Y. Morel (1983) *Remote Assessment of Ocean Color for Interpretation of Satellite Visible Imagery: A Review*. Springer, New York, 114 pp.
- Gordon H. R., O. B. Brown, R. H. Evans, J. W. Brown, R. C. Smith, K. S. Baker and D. K. Clark (1988) A semi-analytic radiance model of ocean color. *Journal of Geophysical Research*, **93**, 10,909–10,924.
- Hoge F. E., A. Vodacek and N. V. Blough (1993) Inherent optical properties of the ocean: Retrieval of the absorption coefficient of chromophoric dissolved organic matter from fluorescence measurements. *Limnology and Oceanography*, **38**, 1334–1402.
- Iturriaga R. and D. A. Siegel (1989) Microphotometric characterization of phytoplankton and detrital absorption properties in the Sargasso Sea. *Limnology and Oceanography*, **34**, 1706–1726.
- Jerlov N. G. (1976) *Marine Optics*. Elsevier, Amsterdam, The Netherlands, 229 pp.
- Kiefer D. A. and J. B. Soohoo (1982) Spectral absorption by marine particles of coastal waters of Baja California. *Limnology and Oceanography*, **27**, 492–499.
- Kirk J. T. O. (1994a) *Light and Photosynthesis in Aquatic Ecosystems*. 2nd edn, Cambridge Univ. Press, Cambridge, U.K., 509 pp.
- Kirk J. T. O. (1994b) Optics of UV-B radiation in natural waters. *Archiv fur Hydrobiologie*, **43**, 1–16.
- Kishino M., C. R. Booth and N. Okami (1984) Underwater radiant energy absorbed by phytoplankton, detritus, dissolved organic matter, and pure water. *Limnology and Oceanography*, **29**, 340–349.
- Knap A. H. *et al.* (1993) BATS Methods—March 1993, BATS Method Manual Version 3, U.S. JGOFS Planning and Coordination Office, Woods Hole, MA, 108 pp.
- Lorenzen C. L. (1972) Extinction of light in the ocean by phytoplankton. *Journal du Conseil International d'Exploration de la Mer*, **34**, 262–267.
- Malin G., S. M. Turner and P. S. Liss (1992) Sulfur: The plankton/climate connection. *Journal of Phycology*, **28**, 590–597.
- Marshall B. R. and R. C. Smith (1990) Raman scattering and in-water ocean optical properties. *Applied Optics*, **29**, 71–84.
- Michaels A. F., A. H. Knap, R. L. Dow, K. Gundersen, R. L. Johnson, J. Sorensen, A. Close, G. A. Knauer, S. E. Lohrenz, V. A. Asper, M. Tuel and R. R. Bidigare (1994) Seasonal patterns of ocean biogeochemistry at the U.S.-JGOFS Bermuda Atlantic Time series Study site. *Deep-Sea Research I*, **41**, 1013–1038.
- Morel A. (1988) Optical modeling of the upper ocean in relation to its biogenous matter content (Case I waters). *Journal of Geophysical Research*, **93**, 10,749–10,768.
- Morel A. (1991) Light and marine photosynthesis: a spectral model with geochemical and climatological implications. *Progress in Oceanography*, **26**, 263–306.
- Morel A. and B. Gentilli (1991) Diffuse reflectance of oceanic waters: its dependence on sun angle as influenced by the molecular scattering contribution. *Applied Optics*, **30**, 4427–4438.
- Morel A. and D. Antoine (1994) Heating rate within the upper ocean in relation to its bio-optical state. *Journal of Physical Oceanography*, **24**, 1652–1665.
- Morrow J. H., W. S. Chamberlin and D. A. Kiefer (1989) A two-component description of spectral absorption by marine particles. *Limnology and Oceanography*, **34**, 1500–1509.
- Mueller J. L. and R. W. Austin (1992) *Ocean optics protocols*. Vol. 5, S. B. Hooker and E. R. Firestone, editors, NASA Tech Memo. 104566, 45 pp.
- Mueller J. L., J. McLean and B. C. Johnson (1993) *The first SeaWiFS intercalibration round-robin experiment, SIRREX-1, July 1992*. Vol. 14, S. B. Hooker and E. R. Firestone, editors, NASA Tech Memo. 104566, 58 pp.

- Nelson J. R. and C. Y. Robertson (1993) Detrital spectral absorption: Laboratory studies of visible light effects on phytodetritus absorption, bacterial spectral signal, and comparison to field measurements. *Journal of Marine Research*, **51**, 181–207.
- Nelson N. B., B. B. Prézelin and R. R. Bidigare (1993) Phytoplankton light absorption and the package effect in California coastal waters. *Marine Ecology Progress Series*, **94**, 217–224.
- Prieur L. and S. Sathyendranath (1981) An optical classification of coastal and oceanic waters based on the specific spectral absorption curves of phytoplankton pigments, dissolved organic matter, and other particulate materials. *Limnology and Oceanography*, **26**, 671–689.
- Roesler C. S., M. J. Perry and K. L. Carder (1989) Modeling in-situ phytoplankton absorption from total absorption spectra in productive inland marine waters. *Limnology and Oceanography*, **34**, 1510–1523.
- Sathyendranath S. and T. Platt (1988) The spectral irradiance field at the surface and in the interior of the ocean: A model for applications in oceanography and remote sensing. *Journal of Geophysical Research*, **93**, 9270–9280.
- Seckel G. R. and F. H. Beaudry (1973) The radiation from the sun and sky over the North Pacific Ocean. (abstract only). *Transactions of the American Geophysical Union*, **54**, 1114.
- Siegel D. A. and T. D. Dickey (1987a) Observations of the vertical structure of the diffuse attenuation coefficient spectrum. *Deep-Sea Research*, **34**, 547–563.
- Siegel D. A. and T. D. Dickey (1987b) On the parameterization of irradiance for open ocean photoprocesses. *Journal of Geophysical Research*, **92**, 14,648–14,662.
- Siegel D. A., C. R. Booth and T. D. Dickey (1986) Effects of sensor characteristics on the inferred vertical structure of the diffuse attenuation coefficient spectrum. *Proceedings of the Society of Photo-Optical Instrumentation Engineers, Ocean Optics VIII*, **637**, 115–123.
- Siegel D. A., A. F. Michaels, J. C. Sorensen, M. O'Brien and M. A. Hammer (1995a) Seasonal variability of light availability and utilization in the Sargasso Sea. *Journal of Geophysical Research*, **100**, 8675–8713.
- Siegel D. A., D. Konnoff, M. C. O'Brien, J. Sorensen and E. Fields (1995b) *BBOP sampling and data processing protocols*. U.S. JGOFS Planning Report Number 19, U.S. JGOFS Planning and Coordination Office, Woods Hole Oceanographic Institution, Woods Hole, MA, 77 pp.
- Sikorski R. L. and R. G. Zika (1993) Modeling mixed-layer photochemistry of H<sub>2</sub>O<sub>2</sub>-optical and chemical modeling of production. *Journal of Geophysical Research*, **98**, 2315–2328.
- Smith R. C. and K. S. Baker (1978a) The bio-optical state of ocean waters and remote sensing. *Limnology and Oceanography*, **23**, 247–259.
- Smith R. C. and K. S. Baker (1978b) Optical classification of natural waters. *Limnology and Oceanography*, **23**, 260–267.
- Smith R. C. and K. S. Baker (1981) Optical properties of the clearest natural waters. *Applied Optics*, **20**, 177–184.
- Smith R. C., C. R. Booth and J. L. Star (1984) Oceanographic bio-optical profiling system. *Applied Optics*, **23**, 2791–2797.
- Smith R. C., J. Marra, M. J. Perry, K. S. Baker, E. Swift, E. Buskey, D. A. Kiefer (1989) Estimation of a photon budget for the upper ocean in the Sargasso Sea. *Limnology and Oceanography*, **34**, 1677–1697.
- Sooahoo J. B. and D. A. Kiefer (1982) Vertical distribution of phaeopigments—I. A simple grazing and photooxidative scheme for small particles. *Deep-Sea Research*, **29**, 1539–1551.
- Sorensen J., D. Konnoff, M. C. O'Brien, E. Fields and D. A. Siegel (1994). The BBOP data processing system. In: *Ocean Optics XII, Proceedings of the Society of Photo-optical Instrument Engineers*, **2258**, 539–546.
- Stavn R. H. and A. D. Weidemann (1992) Raman scattering in ocean optics—quantitative assessment of internal radiant emission. *Applied Optics*, **31**, 1294–1303.
- Vernet M. and C. J. Lorenzen (1987) The presence of chlorophyll *b* and the estimation of phaeopigments in marine phytoplankton. *Journal of Plankton Research*, **9**, 255–265.
- Walsh J. J., K. L. Carder, F. H. Muller-Karger (1992) Meridional fluxes of dissolved organic matter in the North Atlantic Ocean. *Journal of Geophysical Research*, **97**, 15,625–15,637.
- Weir C. T., D. A. Siegel, A. F. Michaels and D. W. Menzies (1994) An in-situ evaluation of a ship's shadow, In: *Ocean Optics XII, Proceedings of the Society for Photo-optical Instrumentation in Engineering*, **2258**, 815–821.
- Weiss P. S., S. S. Andrews, J. E. Johnson and O. C. Zafriou (1995) Photoproduction of Carbonyl Sulfide in South Pacific Ocean waters as a function of irradiation wavelength. *Geophysical Research Letters*, **22**, 215–218.
- Zika R. G., P. J. Milne and O. C. Zafriou (1993) Photochemical studies of the eastern Caribbean—An introductory overview. *Journal of Geophysical Research*, **98**, 2223–2232.